Palaeo- and rock-magnetic investigations across Jurassic-Cretaceous boundary at St Bertrand's Spring, Drôme, France: applications to magnetostratigraphy

Tiiu Elbra[1], Petr Schnabl[1], Kristýna Čížková[1], Petr Pruner[1], Šimon Kdýr[1], Jacek Grabowski[2], Daniela Reháková[3], Andrea Svobodová[1,4], Camille Frau[5] and William A.P. Wimbledon[6]

1 Institute of Geology of the Czech Academy of Sciences, Rozvojová 269, 165 00 Prague 6, Czech Republic (elbra@gli.cas.cz)

2 Polish Geological Institute - National Research Institute, Rakowiecka 4, 00-975 Warsaw, Poland

3 Department of Geology and Palaeontology, Faculty of Natural Sciences, Comenius University, Mlynská dolina, Ilkovičova 6, SK84215 Bratislava, Slovak Republic

4 Institute of Geology and Palaeontology, Faculty of Science, Charles University, Albertov 6, 128 43 Prague 2, Czech Republic

5 Groupement d'Intérêt Paléontologique, Science et Exposition, 60 bd. Georges Richard, 83000 Toulon, France

6 School of Earth Sciences, University of Bristol, Queens Road, Bristol BS8 1RJ, U.K.

Received: January 6, 2017; Revised: May 31, 2017; Accepted: August 8, 2017

ABSTRACT

Palaeo- and rock-magnetic investigations of the St Bertrand's Spring (Le Ravin de Font de St Bertrand) locality in France were carried out in order to contribute to, and improve, the stratigraphy of the Jurassic-Cretaceous boundary interval. Magnetic susceptibility shows slightly diamagnetic behaviour in the lowermost part of the profile and an increase (paramagnetic) towards its middle and upper parts. Rock-magnetic measurements throughout the section show magnetite as the main magnetic fraction, together with traces of hematite. Additionally, thermal demagnetization indicates the presence of goethite. Our magnetostratigraphy indicates three normal/reversed polarity sequences; possibly encompassing the magnetozones M19r to the M17n. This suggests that the St Bertrand section straddles the Tithonian/Berriasian boundary and reaches the middle Berriasian sensu lato.

Keywords: rock magnetism, magnetostratigraphy, Jurassic-Cretaceous boundary, palaeomagnetism, St Bertrand

© 2018 Inst. Geophys. CAS, Prague

1. INTRODUCTION

The Jurassic-Cretaceous (J-K) transition has puzzled the stratigraphic community for generations. Due to the extreme heterogeneity of facies and biota, the effect of global sea level change and regression, and high provincialism - the major ocean of Tethys, where most J-K studies have been focussed, had only transient or no connections with boreal and austral regions; the global definition of a J-K boundary has been difficult to distinguish (*Wimbledon et al., 2011*). Improving correlations in the J-K boundary interval in Tethys, as well as providing better correlations between Tethys and high-latitude regions, and non-marine areas, has been the focus of the Berriasian Working Group (BWG) since 2008 (*Wimbledon et al., 2013*; *Michalík et al., 2016*; *Wimbledon, 2014*).

Biostratigraphy has made significant advances, notably with calpionellids, and an easily recognizable magnetozone pattern across the J-K boundary interval has been identified in biostratigraphically calibrated sections mostly in (i) Tethyan marine profiles in Austria (*Lukeneder et al., 2010*), Crimea (*Guzhikov et al., 2012*), France (*Wimbledon et al. 2013*), Hungary (*Grabowski et al., 2010a*), Italy (*Houša et al., 2004*; *Ogg and Lowrie, 1986*; *Channell et al., 2010*; *Ogg et al., 1991*; *Satolli et al., 2015*), Slovakia (*Houša et al., 1999*; *Michalík et al., 2009, 2016*; *Grabowski et al., 2010b*), Poland *(Grabowski and Pszczółkowski, 2006*), Spain (*Ogg et al., 1984*; *Pruner et al., 2010*), but also (ii) in the Boreal: Nordvik, N. Siberia (*Houša et al., 2007*; *Bragin et al., 2013*; *Dzyuba et al., 2013*; *Guzhikov, 2013*; *Zakharov et al., 2014*), as well as non-marine facies (*Ogg et al., 1991*). Even though the base of the *Alpina* Subzone has now been fixed by the BWG to be the primary marker for the J-K boundary, magnetostratigraphy remains an indispensable tool in providing worldwide correlations around the boundary.

To better document sequences that cross the system boundary, further determine the boundaries of magnetozones and the thin reversed subzones, and contribute to global definition of the J-K boundary, several ‘old’ and ‘new’ marine profiles across the Europe have been (re)visited. This paper presents palaeo- and rock-magnetic research results from an ‘old’ Drôme ammonite locality, but one never before studied for palaeomagnetism: Le Ravin de Font de St Bertrand (St Bertrand’s Spring, hereafter called St Bertrand).

2. St BERTRAND SECTION

The St Bertrand locality (Fig. 1; longitude 5°37′00″E, latitude 44°42′09″N; Les Combes in *Frau et al., 2016a*) is situated north of the hamlet of Les Combes, in a cliffed upper valley of the Grimone stream, on the northern side of the Ravin de St Bertrand’s Spring. The section is almost 60 m thick and consists of three lithological parts. (i) Stacked lime-mud to wackestone-limestones make up the lower part of the section. According to *Frau et al. (2016a) Delphinella delphinense* and *Proniceras pronum* appear in the upper portion of this interval. The lowermost part is followed by (ii) well-bedded, ammonite-bearing limestones with thin marly interbeds. The lower portion of the interval is dominated by *Pseudosubplanites*. *Strambergella carpathica* and *Strambergella jacobi* occur in the upper part of this zone and correlate well with the lowermost *Calpionella elliptica* Subzone and uppermost *Remaniella ferasini* Subzone of the standard *Calpionella* Zone (*Frau et al., 2016a*). (iii) The upper half of St Bertrand section comprises continuous marl-limestone alternations.

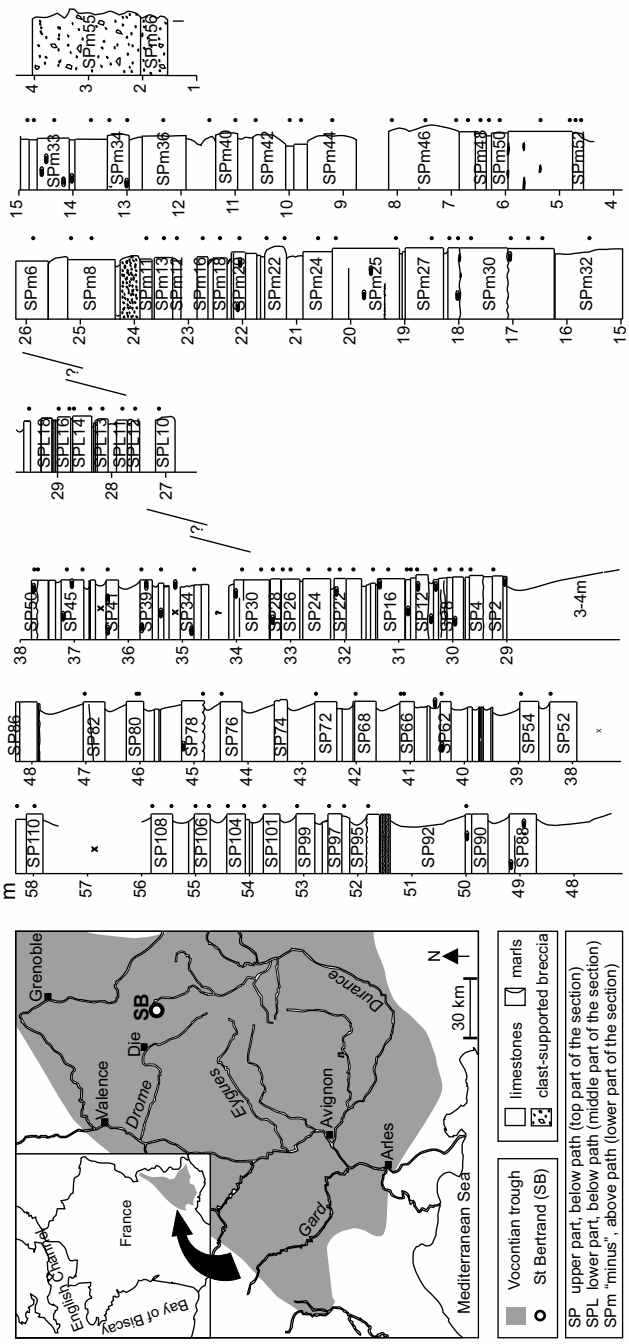

Fig. 1. The location and lithology of St Bertrand section. Position of samples is marked with black dots in the lithological column.

Regionally, the St Bertrand site is a part of the succession of the Vocontian trough (see *Wimbledon et al., 2013*). A sequence of deeper-water pelagic and hemipelagic sediments are found in the Jurassic-Cretaceous transition with alternating periods of marl and limestone deposition. In some areas, particularly in the north, it contains marginal marine or terrestrial Purbeck facies (*Détraz and Mojon, 1989*; *Wimbledon et al., 2013*). The sedimentation of the basin was restricted by the Cévennes massif in the west and Les Maures in the south. Eastwards the basin was open to the ocean of Tethys.

3. SAMPLING AND METHODS

Pilot sampling of the St Bertrand section was carried out in two stages: the samples from upper part (SP) and middle part (SPL) were collected in 2011, and lower part (SPm) in 2015 (Fig. 2). Additional sampling was undertaken in autumn 2016 to fill in the data gaps and verify the preliminary results. Only limestones were collected and recorded by bed number (Fig. 1). The vertical scale (as in *Frau et al., 2016a*) starts at the bottom of the section, below the first prominent bedded layer (0.5 m thick). Below that, the rocks are profoundly shattered and weathered with no detectable bedding structure.

Each sample was prepared as several cylindrical (diameter of 2.5 cm) or cubic (8 cm^3) specimens and subjected to palaeo- and rock-magnetic investigations in the Laboratory of Palaeomagnetism, Institute of Geology of the Czech Academy of Sciences.

The progressive thermal (TD) demagnetization, from 80°C to 560°C (occasionally 640°C) in 40°C intervals, was carried out using the MAVACS (Magnetic Vacuum Control System; *Příhoda et al., 1989*). The remanence (e.g., natural remanent magnetization *NRM*) was measured using a 2G Superconducting Rock Magnetometer 755 (2G SRM). The magnetic susceptibility (κ) was measured with an AGICO KLF–4A Automatic Magnetic Susceptibility Meter after each demagnetizing step. Alternating field (AF) demagnetization, up to 100 mT in 5–10 mT intervals, was carried out using a 2G SRM. Results derived from the palaeomagnetic measurements were analysed with Remasoft software (*Chadima and Hrouda, 2006*).

Rock-magnetic measurements, e.g., temperature dependence of mass-specific magnetic susceptibility (χ-*T*) and acquisition of isothermal remanent magnetization (*IRM*), were carried out on selected samples. The temperature dependence of magnetic susceptibility was measured using an AGICO MFK1 kappabridge. Measurements were carried out in an argon atmosphere over a temperature range of –192° to 700°C. After AF demagnetization, several samples were also progressively magnetized up to 1 T or 2 T using a Magnetic Measurements pulse magnetizer (MMPM10) and then stepwise demagnetized ($\leq$ 100 mT) using a LDA-3. The resulting saturation remanent magnetization was measured with an AGICO JR-5 spinner magnetometer.

4. RESULTS

The magnetic susceptililities (κ) and natural remanent magnetization (*NRM*) of the St Bertrand specimens are presented in Fig. 3 and average values of each sample bed summarized in Table 1. Based on measured data, the lowermost part (SPm; 0–20 m) of the section shows mainly diamagnetic behaviour, whereas the rest of the section (SP and

SPL) consists of paramagnetic samples (Fig. 3). Additionally, the frequency dependence of magnetic susceptibility (FD) was measured; however, the samples are not sufficiently strong to gain enough reliable FD results.

Curie temperatures (T_C) were determined from temperature-dependent measurements of the mass-specific magnetic susceptibility (χ-T curves) (Fig. 4). Throughout the sequence rock-magnetic properties show magnetite (T_C: 450–580°C) as the main

Fig. 2. Examples of the upper (SP), middle (SPL) and lower (SPm) part of St Bertrand section. SPL part of the section got recently destroyed.

magnetic fraction. Many χ-T curves indicate also a minor fraction with T_C over 600°C, which is typical for a hematite-like phase, and in few specimens a fraction with $T_C \sim 300–350$°C. The latter can be an indicator of several minerals, including sulphides, maghemites, titano-magnetites. One sample has a heating curve (Fig. 4 right) that indicates also a fraction with a possible T_C over the measured temperature range (700°C). The Verwey transition was not observed in any samples. The χ in low temperatures decreased until −80°C, after which it increased again until room temperature close to its initial value. All samples display irreversible behaviour in their heating-cooling cycles, with formation of new magnetite or a magnetite-like phase ($T_C \sim 450–590$°C; Fig. 4), in some case also a fraction that has a T_C over 600°C.

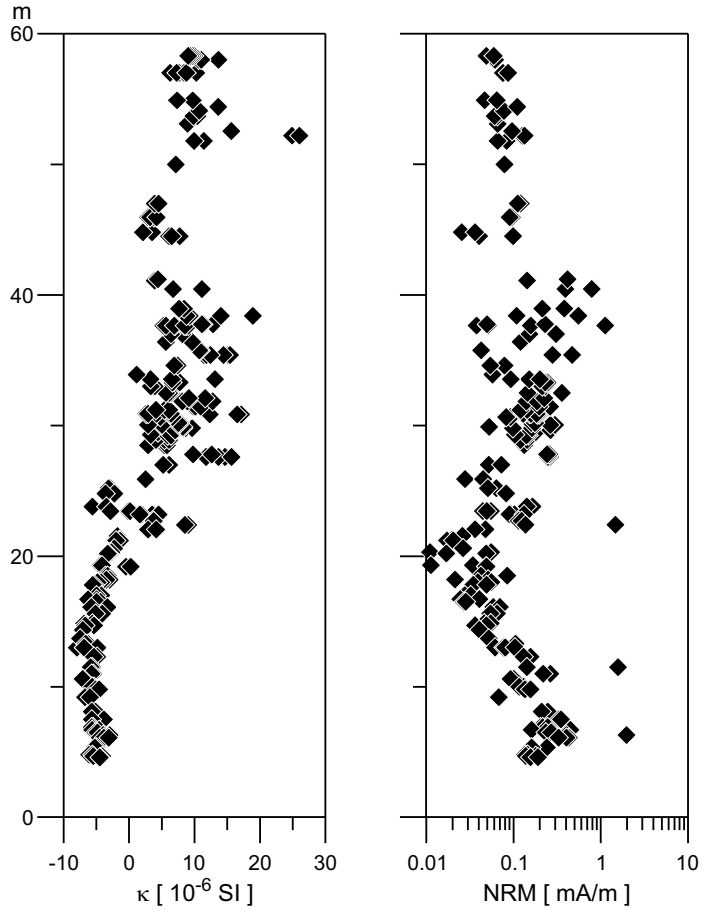

Fig. 3. Magnetic susceptibilities (κ) and natural remanent magnetization (*NRM*) of the St Bertrand section.

Table 1. Average values of magnetic susceptibility (κ) and natural remanent magnetization (*NRM*) of the St Bertrand section. Only limestones were sampled. *n* - number of specimens.

Sample	Lithology (*Frau et al., 2016*)	*n*	κ [10^{-6} SI]	*NRM* [mA/m]	Sample	Lithology (*Frau et al., 2016*)	*n*	κ [10^{-6} SI]	*NRM* [mA/m]
SP111	1. continuous marl - limestone alternations	4	9.45	0.05	SP006	2. ammonite-bearing limestones with thin marly interbeds	4	9.00	0.13
SP110		3	11.75	0.06	SP004		1	7.00	0.26
SP109		6	8.08	0.08	SP003		1	3.30	0.10
SP106		2	8.50	0.06	SP002		2	6.13	0.14
SP104		2	12.15	0.09	SPL18		2	4.38	0.16
SP101		2	10.10	0.06	SPL16		3	5.20	0.13
SP099		1	8.90	0.07	SPL14		3	4.67	0.13
SP097		1	15.60	0.10	SPL12		4	13.91	0.25
SP096		2	25.44	0.13	SPL11		2	11.19	0.25
SP094		2	10.65	0.07	SPL10		2	5.65	0.06
SP091		1	7.13	0.08	SPm06		2	2.56	0.04
SP082		2	4.19	0.12	SPm08		4	–2.99	0.07
SP080		4	3.53	0.09	SPm11		2	–4.56	0.15
SP078		2	2.80	0.03	SPm13		3	–0.95	0.05
SP076		3	6.77	0.07	SPm14		5	3.05	0.10
SP066		2	4.13	0.28	SPm16		2	3.75	0.12
SP062		2	8.90	0.59	SPm18		2	8.75	0.80
SP054		2	8.00	0.30	SPm20		2	3.50	0.04
SP052		4	12.72	0.33	SPm22		4	–1.68	0.02
SP050		3	11.73	0.14	SPm24		1	–2.30	0.03
SP049		8	7.42	0.34	SPm25		8	–2.61	0.03
SP045		2	7.25	0.23	SPm27		2	–3.46	0.06
SP041		1	7.60	0.12	**Average**			**4.74**	**0.14**
SP039		2	10.80	0.04	SPm29	3. stacked - mud - to wackestone – limestones	4	–3.90	0.04
SP037		6	13.42	0.37	SPm30		8	–5.10	0.03
SP032		2	7.13	0.07	SPm32		4	–4.60	0.06
Average			**9.29**	**0.17**	SPm33		6	–6.53	0.05
SP030	2. ammonite-bearing limestones with thin marly interbeds	4	5.99	0.13	SPm34		6	–6.59	0.09
SP028		3	7.23	0.24	SPm36		2	–5.14	0.14
SP026		2	3.60	0.22	SPm39		2	–5.75	0.86
SP024		4	6.13	0.25	SPm40		2	–5.63	0.24
SP022		2	10.36	0.22	SPm42		6	–5.81	0.12
SP021		3	9.92	0.16	SPm44		2	–6.38	0.07
SP018		4	10.20	0.23	SPm46		7	–5.34	0.26
SP016		3	5.20	0.13	SPm47		2	–5.12	0.30
SP015		7	4.97	0.16	SPm48		2	–4.99	0.25
SP014		3	15.30	0.19	SPm49		2	–3.50	1.18
SP012		2	5.69	0.09	SPm50		3	–3.83	0.39
SP009		2	7.63	0.17	SPm51		4	–5.50	0.17
SP008		3	5.13	0.28	SPm52		4	–4.63	0.17
SP007		1	8.20	0.05	**Average**			**–5.31**	**0.19**

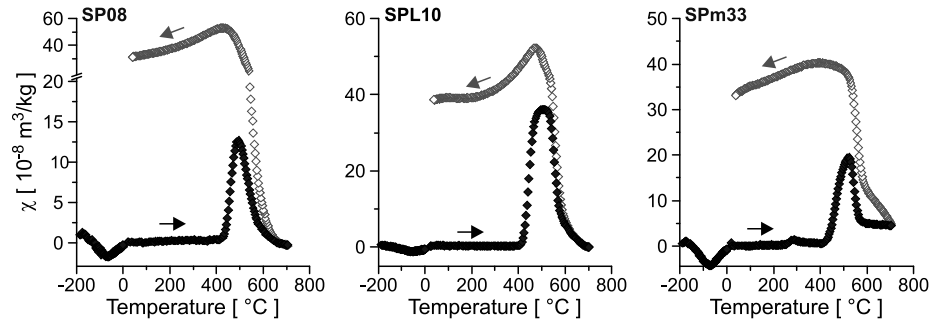

Fig. 4. Examples of temperature dependence of magnetic susceptibility for upper (SP08), middle (SPL10) and lower (SPm33) part of St Bertrand section.

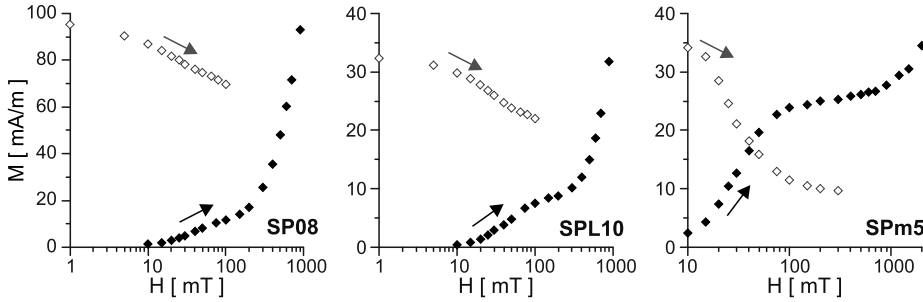

Fig. 5. Examples of acquisition (full symbols) and demagnetization (open symbols) of isothermal remanence for upper (SP8), middle (SPL10) and lower (SPm50) part of St Bertrand section.

The determined remanence values show generally low *NRM* through the entire St Bertrand profile (Fig. 3). The *NRM* values decrease in the lowest beds as well as in the upper part (between 0 and 20 m and 40 and 60 m, respectively), with an increasing trend within the 20–40 m interval.

The acquisition of isothermal remanence (Fig. 5) indicates 2 distinct magnetic fractions: of low and high coercivity. The first fraction gains its saturation by 100 mT, which is typical behaviour for magnetite, whereas the second (magnetic saturation not reached by 1–2 T) may indicate either goethite (the possible carrier of TD low temperature remanence; Fig. 6) or hematite (seen in χ-T curves; Fig. 4). Additional Lowrie test (*Lowrie, 1990*) indicates the presence of magnetite, hematite and, occasionally, goethite.

AF demagnetization of the samples showed that remanence of the SPm is mostly completely removed by 50 mT (medium demagnetizing field < 10 mT), which indicates that the low coercivity fraction, such as magnetite, is the carrier of the remanence. Occasionally ≥ 20% of remanence remains by 100 mT. However, samples from the upper part of the sequence are (with exception of samples in the 29–32 m interval) more resistant to alternating field and are not demagnetized by 100 mT (≥ 40% of remanence

remains and, hence, AF data is not here used in the component analysis and magnetostratigraphy). This is possibly due to high coercivity minerals, such as goethite or hematite. Thermal demagnetization (TD; Fig. 6b) of the samples establishes that most of the remanence is removed between 100 and 300°C, occasionally also by temperatures up to 500°C (especially in the lowest 11 m of the section; samples SPm39-50). A shallow increase and consequent decrease of magnetization occurs within the 200–600°C interval, showing the presence of a remanence component carried by magnetite throughout the section. In most samples, the changes in mineral phase, as displayed by the rise of magnetic susceptibility, occur between 300–500°C in SPm and above 500°C in SPL and SP.

Characteristic remanent magnetization (*ChRM*; Fig. 6a) was determined using principal component analysis (PCA) (after *Kirschvink, 1980)*. On average, the *ChRM* occurs within temperature range of 280–500°C (5–8 steps; occasionally up to 600°C) for reversed polarity and 160–360°C (4–6 steps; occasionally up to 520°C) for the normal polarity component. The difference in temperature range of *ChRM* is caused by the presence of additional low temperature (up to 240°C) B-component in the reversed polarity samples. This component (declination $D = 3°$, inclination $I = 65°$; *in situ* coordinates) is very close to the present earth field for this locality. The palaeomagnetic results (Table 2) of 46 samples with normal polarity and 33 reversed, out of 250 specimens, were combined to construct a magnetostratigraphy. All the AF demagnetized specimens were disregarded because of their potential content of secondary goethite (see above). Many TD specimens had remanent magnetization that was too low or unstable to be interpreted correctly and, hence, these were also discarded. Furthermore, approximately 20 of the TD specimens were not used because of the low intensity of their signal, increase of κ during the thermal treatment or sample disintegration in the oven, and 27 samples could be interpreted, but only by using the *Fischer (1953)* mean above 320°C.

Three normal and three reverse polarity zones have been identified (Fig. 7). The first magnetozone (Mz1r) is based on only 2 specimens, the component was counted using the *Fisher (1953)* mean and the 95% confidence angle α_{95} exceeds 20°. The next magnetozone (Mz1n) is approximately 20 m in thickness. The lower part is composed of several 'well behaved' samples, with relatively high magnetization, and low maximum angular deviation (*MAD*). However, the upper part of the zone consists of samples with very weak remanent magnetization and an increasing κ in the high temperatures. This causes uncertainties in interpretation, and therefore we mark the interval in grey. Magnetozone Mz2r is based on 4 specimens (mean directions calculated, as above, by the Fisher mean). The next magnetozone (Mz2n) starts with samples that have normal polarity, but ends with a long transitional interval where the polarity seemingly changes several times due to low and unstable primary magnetization (grey interval in Fig. 7). The upper magnetozones (Mz3r and Mz3n) comprise samples with higher remanent magnetization and a low *MAD* angle. Mz3r contains three samples with the negative magnetic inclination and a magnetic declination facing north, and one normally magnetized sample that we decided to disregard in further evaluation.

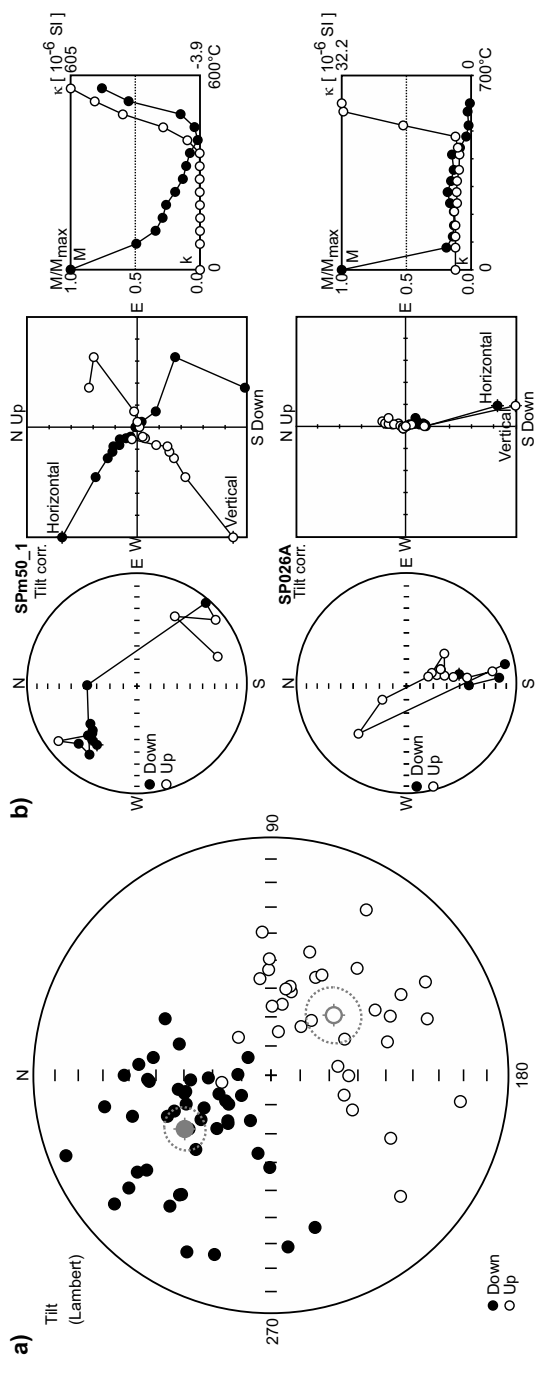

Fig. 6. **a)** Stereographic projection of normal and reversed characteristic remanent magnetization (*ChRM*) components (full and open symbols, respectively). The average *ChRM* for both components and their confidence intervals are displayed in grey. **b)** Examples of thermal demagnetization data: stereographic projection (left), Orthogonal (Zijderveld) vector projection (middle), and magnetization and susceptibility intensity curves (right). In the stereoplots the open/full symbols indicate the projection in the upper/lower hemisphere, respectively. In the Zijderveld plots open/full symbols indicate the projection on the vertical/horizontal plane, respectively.

Table 2. Palaeomagnetic data of the St Bertrand section. D - declination; I - inclination; α_{95} - 95% confidence limit; k - precision parameter; n - number of specimens; T - average temperature range of characteristic remanent magnetization; N - normal polarity; R - reversed polarity.

Polarity	Structural Tilt Correction				No Structural Tilt Correction (*In Situ* Directions)				n	T [°C]
	Mean Directions		α_{95} [°]	k	Mean Directions		α_{95} [°]	k		
	D [°]	I [°]			D [°]	I [°]				
N	329.1	54.8	7.1	9.79	13.8	51.0	6.6	11.13	46	160–360
R	135.3	–58.8	9.2	8.32	178.5	–48.2	8.2	10.23	33	280–500

The sampled beds in St Bertrand are tilted without folding. However, the bedding surfaces undulate and this lead to lower precision when measuring the dip of the strata. As a result, the angle α_{95} for the tilt-corrected data is slightly larger than that from *in-situ* coordinates. For all the normally and reversely polarized samples, the angle between the Fisher mean is 171.1°, and the directions of samples are antipodal. The angle between estimated mean vectors is 8.5°, compared with the critical value 11.4°, estimated using the hypothesized Fisher distribution. The palaeomagnetic data passed the reversal test and was classified as C according to the method of *McFadden and McElhinny (1990)*.

5. DISCUSSION

A detailed ammonite distribution together with preliminary results on the calpionellid zonation for St Bertrand is given in *Frau et al. (2016)*. These data indicate that base of the *Calpionella alpina* Subzone lies in the middle of our magnetozone Mz1n. Furthermore, the first appearance of the calcareous nannofossil species *Nannoconus wintereri* occurs within this interval. This suggests that the magnetozone Mz1n could be either the M19n or M19n.2n. Comparison with other sections (Fig. 8) shows that the J-K boundary according to calpionellids (base of *Alpina* Subzone) and nannoplankton (FO of *Nannoconus wintereri*) is usually in the middle of normal polarity zone (M19n2n). As further evidence, M19n.2n records the acme of the ammonite genus *Delphinella* at Le Chouet, as at St Bertrand (*Frau et al., 2016a, b*). In the lowest part of the St Bertrand section, there are two samples that seemingly have reversed polarity. Based on the identification of Mz1n zone as M19n (see above), we believe that Mz1r corresponds to the top of the reversed zone M19r. Comparison of the rest of the site's pattern of magnetozones (Mz2r-Mz3n) with the Geomagnetic Polarity Time Scale (GPTS) and with preliminary calpionellid stratigraphy (e.g., placement of *Ferasini*/*Elliptica* Subzones (*Frau et al., 2016a*; Fig. 8)) reveals that the long reversed zone Mz3r can be only M17r. The interpretation is supported by situation of the *B. jacobi/T. occitanica auctorum* ammonite zonal boundary in this magnetozone (*Frau et al., 2016a*; *Gradstein et al., 2012*). According to our observations the base of *Elliptica* Subzone probably occurs slightly lower than reported by *Frau et al. (2016a)*. To verify both the lower and upper boundary of this subzone

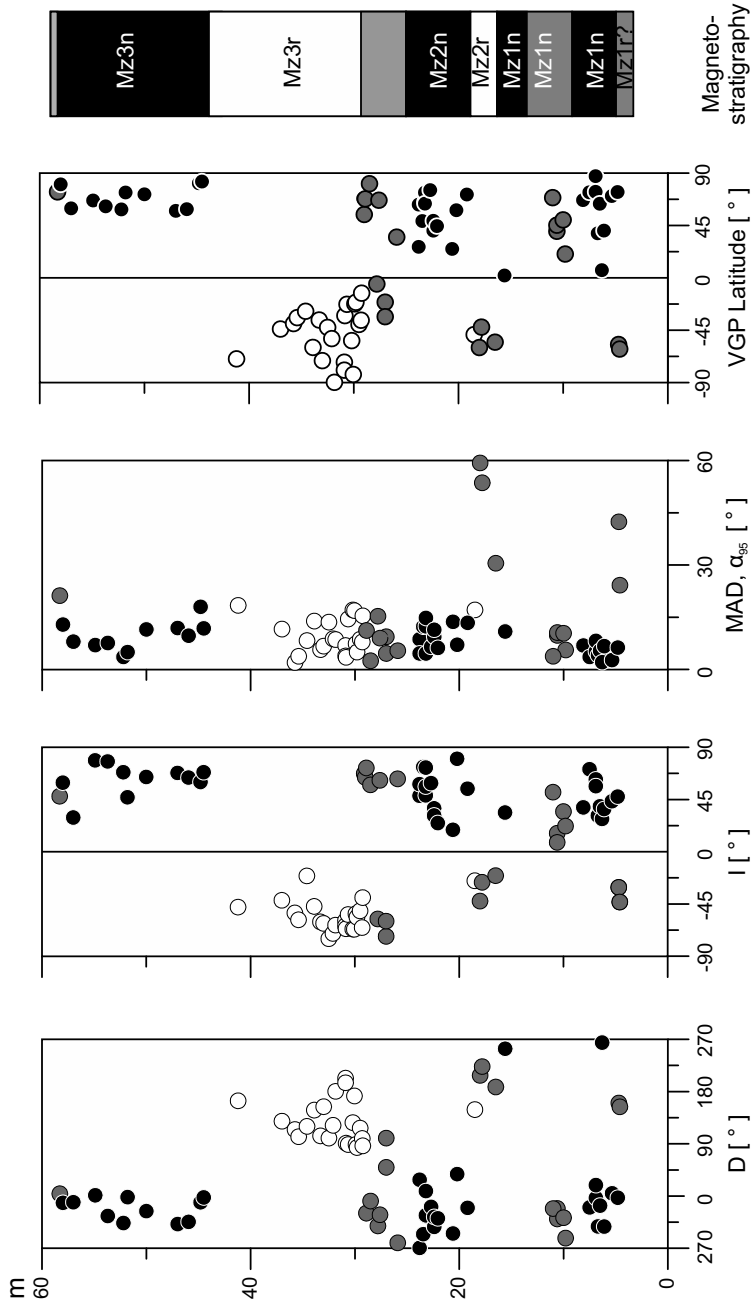

Fig. 7. Declination (*D*), inclination (*I*), maximum angular deviation (*MAD*) or 95% confidence angle (α_{95}), VGP latitude and magnetostratigraphy at St Bertrand section. Full/open symbols denote normal/reversed polarities, respectively. Grey symbols represent specimens with either high *MAD* (or α_{95} for samples where *ChRM* was calculated using Fisher statistics) or which are from areas with unclear magnetostratigraphy.

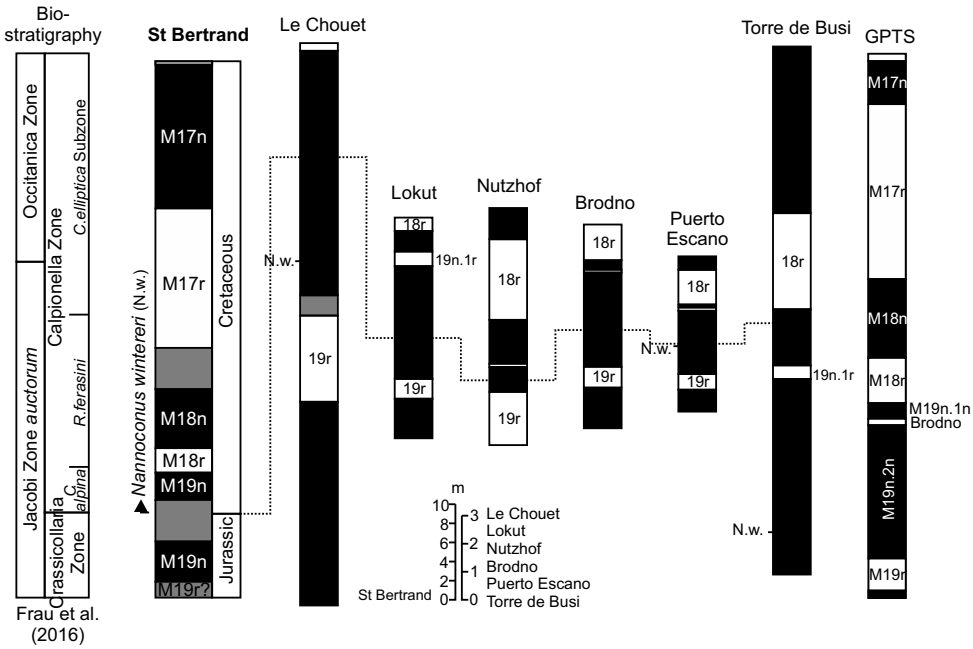

Fig. 8. Magnetostratigraphy (current work) and biostratigraphy (after *Frau et al., 2016*) of St Bertrand section, and comparison with other European sections (redrawn after *Wimbledon et al., 2011*) and with Geomagnetic Polarity Time Scale (GPTS; after *Gradstein et al., 2012*).

the new samples have been collected. Thus, the St Bertrand section most probably contains magnetozones from the upper Tithonian (M19r) up to middle Berriasian (M17n). This interpretation implies a large increase of sedimentation rate between magnetozones M17r (10.6–13.7 m/My) and M17n (>39 m/My), which is also visible from the lithological log (Fig. 1) where marl interbed thicknesses increase. The Brodno subzone (M19n.1r) has not been recognized.

Magnetic susceptibility is usually interpreted as a proxy of detrital input towards the basin and, thus, is increasingly used as a palaeoenvironmental and climatic proxy as well as a high resolution intercontinental correlation tool (e.g., *Ellwood et al., 1999*; *Grabowski et al., 2013*; *Da Silva et al., 2013*). Based on our data, magnetic susceptibility (Fig. 3) increases from the lowermost part of the section, of Tithonian age (M19r), to the middle Berriasian. This trend is opposite to that seen in other Tethyan sections. Usually κ decline is observed between the Tithonian and middle Berriasian, and is related to a relative decrease of lithogenic input and increased carbonate productivity (*Houša et al., 1999*; *Grabowski et al., 2010a, 2013*; *Michalík et al., 2016*). The trend of κ in the St Bertrand sequence is rather similar to the trend found in the Hlboča section in the Western Carpathians (*Grabowski et al., 2010b*). At Hlboča, the κ increase is accompanied by presence of superparamagnetic magnetite (*op. cit.*). The increase in κ in the upper part of the St Bertrand's section clearly corresponds to lithological changes, from pure massive

limestones into well-bedded limestones with marl intercalations, and thus a palaeoenvironmental change. As the section exhibits primary magnetization it is rather unlikely that κ is significantly influenced by secondary ferromagnetic minerals. Furthemore, even in partially remagnetized carbonates the κ can still preserve primary paleoenvironmental information (*Da Silva et al., 2013*). It should be noted that our study is the first detailed κ record in the middle Berriasian of the Vocontian Basin. The nearby Le Chouet section terminates in M19n, still in the *Alpina* Subzone (*Wimbledon et al., 2013*). Therefore, it is not clear whether the κ increase between magnetozones M19n and M17r-M17n is a regional trend characteristic for the entire Vocontian Basin or that it represents just a local feature. Significant intensification of terrigenous input in the Vocontian Basin is usually observed higher in the Berriasian in calpionellid zone D (*Calpionellopsis* Zone) (*Morales et al., 2013*).

6. CONCLUSIONS

The magnetostratigraphy of the St Bertrand section documents three normal/reversed polarity zones which have upper Tithonian (M19r) to middle Berriasian (M17n) ages. Magnetic susceptibility shows an increasing trend from the Tithonian into the Berriasian, contrary to other Tethyan sections. Based on rock-magnetic measurements, magnetite is shown to be the main magnetic mineral and carrier of characteristic remanence components throughout the sequence. Goethite and/or traces of hematite are also found. The new data obtained during this study in combination with biostratigraphy (combining 4 major markers of the J-K boundary: magnetostratigraphy, calpionellids, nannoplankton, and ammonites), gives new insights into the J-K boundary in the Vocontian Basin and, in this way, contributes to the dataset for the definition of a global J-K boundary.

Acknowledgements: We would like to express our gratitude to L.G. Bulot (Aix-Marseille Université/Manchester University) for his help during fieldwork campaigns and J. Petráček for help with sample preparation. We are grateful to two anonymous reviewers for their helpful reviews. This research is supported by Grant Agency of the Czech Republic No. GA16-09979S. The publication is in concordance with research plan of the Institute of Geology of the Czech Academy of Sciences, No. RVO67985831. Identification and evaluation of the calpionellids was funded by grant agency VEGA project No. 2/0057/16.

References

Bragin V.Y., Dzyuba O.S., Kazansky A.Y. and Shurygin B., 2013. New data on the magnetostratigraphy of the Jurassic-Cretaceous boundary interval, Nordvik Peninsula (northern East Siberia). *Russ. Geol. Geophys.*, **54**, 335–348.

Chadima M. and Hrouda, F. 2006. Remasoft 3.0 - a user friendly palaeomagnetic data browser and analyzer. *Travaux Geophysiques*, **XXVII**, 20–21.

Channell J.E.T., Casellato C.E. Muttoni G. and Erba E., 2010. Magnetostratigraphy, nannofossil stratigraphy and apparent polar wander for Adria-Africa in the Jurassic-Cretaceous boundary interval. *Paleogeogr. Paleoclimatol. Paleoecol.*, **293**, 51–75.

Da Silva A.C., De Vleeschouwer D., Boulvain F., Claeys P., Fagel N., Humblet M., Mabille C., Michel J., Sardar Abadi M., Pas D. and Dekkers M.J., 2013. Magnetic susceptibility as a high-resolution correlation tool and as a climatic proxy in Paleozoic rocks - merits and pitfalls: examples from the Devonian in Belgium. *Mar. Pet. Geol.*, **46**, 173–189.

Dzyuba O.S., Izokh O.P. and Shurygin B.N., 2013. Carbon isotope excursions in Boreal Jurassic-Cretaceous boundary sections and their correlation potential. *Paleogeogr. Paleoclimatol. Paleoecol.*, **381**, 33–48.

Ellwood B.B., Crick R.E. and El Hassani A., 1999. Magnetosusceptibility event and cyclostratigraphy (MSEC) method used in geological correlation of Devonian rocks from Anti-Atlas Morocco. *AAPG Bull.*, **83**, 1119–1134.

Fisher R.A., 1953. Dispersion on a sphere. *Proc. R. Soc. London A*, **217**, 295–305.

Frau C., Bulot L.G., Reháková D., Wimbledon W.A.P. and Ifrim C., 2016a. Revision of the ammonite index species *Berriasella jacobi* Mazenot, 1939 and its consequences for the biostratigraphy of the Berriasian Stage. *Cret. Res.*, **66**, 94–114.

Frau C., Bulot L.G., Wimbledon W.A.P. and Ifrim, C., 2016b. Systematic palaeontology of the Perisphinctoidea across the Jurassic/Cretaceous boundary at Le Chouet (Drôme, France) and its biostratigraphic implications. *Acta Geol. Pol.*, **66**, 157–177.

Grabowski J. and Pszczółkowski A., 2006. Magneto- and biostratigraphy of the Tithonian-Berriasian pelagic sediments in the Tatra Mountains (central Western Carpathians, Poland): sedimentary and rock magnetic changes at the Jurassic/Cretaceous boundary. *Cret. Res.*, **27**, 398–417.

Grabowski J., Haas J., Márton E. and Pszczółkowski A., 2010a. Magneto- and biostratigraphy of the Jurassic/Cretaceous boundary in the Lókút section (Transdanubian Range, Hungary). *Stud. Geophys. Geod.*, **54**, 1–26.

Grabowski J., Michalík J., Pszczółkowski A. and Lintnerová O., 2010b. Magneto- and isotope stratigraphy around the Jurassic/Cretaceous boundary in the Vysoká Unit (Male Karpaty Mountains): correlations and tectonic implications. *Geol. Carpath.*, **61**, 309–326.

Grabowski J., Schnyder J., Sobień K., Koptiková L., Krzemiński L., Pszczółkowski A., Hejnar J. and Schnabl P., 2013. Magnetic susceptibility and spectral gamma logs in the Tithonian-Berriasian pelagic carbonates in the Tatra Mts (Western Carpathians, Poland): palaeoenvironmental changes at the Jurassic/Cretaceous boundary. *Cret. Res.*, **43**, 1–17.

Gradstein F.M., Ogg J.G., Schmitz M.D. and Ogg G.M., 2012. *The Geologic Time Scale 2012*. 1st Edition. Elsevier, Oxford, U.K.,144 pp.

Guzhikov A.Y., Arkadiev V.V., Baraboshkin E.Y., Bagaeva M.I., Piskunov V.K., Rud'ko S.V., Perminov V.A. and Manikin A.G., 2012. New sedimentological, bio-, and magnetostratigraphic data on the Jurassic-Cretaceous boundary interval of Eastern Crimea (Feodosiya). *Stratigr. Geol. Correl.*, **20**, 261–294.

Guzhikov A.Y., 2013. Solving unsolvable problems in stratigraphy (Comments on the paper "New data on the magnetostratigraphy of the Jurassic-Cretaceous boundary interval, Nordvik Peninsula (northern east Siberia)" by Bragin, Dzyuba, Kazansky & Shurygin). *Russ. Geol. Geophys.*, **54**, 349–354.

Houša V., Krs M. Krsová M., Man O., Pruner P. and Venhodová D., 1999. High-resolution magnetostratigraphy and micropaleontology across the J/K boundary strata at Brodno near Žilina, western Slovakia: summary of results. *Cret. Res*., **20**, 699–717.

Houša V., Krs M., Man O., Pruner P., Venhodová D., Cecca F., Nardi G. and Piscitello M., 2004. Combined magnetostratigraphic, palaeomagnetic and calpionellid investigations across the Jurassic/Cretaceous boundary strata in the Bosso Valley, Umbria, central Italy. *Cret. Res.*, **25**, 771–785.

Houša V., Pruner P., Zakharov V.A., Kostak M., Chadima M., Rogov M.A., Šlechta S. and Mazuch M., 2007. Boreal-Tethyan correlation of the Jurassic-Cretaceous boundary interval by magneto- and biostratigraphy. *Stratigr. Geol. Correl.*, 15, 3, 297-309.

Kirschvink, J.L., 1980. The least-squares line and plane and the analysis of palaeomagnetic data. *Geophys. J. R. Astron. Soc.*, **62**, 699–718.

Lowrie W., 1990. Identification of ferromagnetic minerals in a rock by coercivity and unblocking temperature properties. *Geophys. Res. Lett.*, **17**, 159–162.

Lukeneder A., Halásová E., Kroh A., Mayrhofer S., Pruner P., Reháková D., Schnabl P., Sprovieri M. and Wagreich M., 2010. Multistratigraphic investigations of the Jurassic-Cretaceous boundary interval in the Gresten Klippenbelt (Austria) - evidence for depositional and evolutionary events. *Geol. Carpath.*, **61**, 365–381.

McFadden P.L. and McElhinny M.W., 1990. Classification of the reversal test in palaeomagnetism. *Geophys. J. Int.*, **103**, 725–729.

Michalík J., Reháková D., Grabowski J., Lintnerová O., Svobodová A., Schlögl J., Sobień K. and Schnabl P., 2016. Stratigraphy, plankton communities, and magnetic proxies at the Jurassic/Cretaceous boundary in the Pieniny Klippen Belt (Western Carpathian, Slovakia). *Geol. Carpath.*, **67**, 303–328.

Michalík J., Reháková D., Halásová E. and Lintnerová O., 2009. The Brodno section - a potential regional stratotype of the Jurassic/Cretaceous boundary (Western Carpathians). *Geol. Carpath.*, **60**, 213–232.

Morales C., Gardin S., Schnyder J., Spangenberg J., Arnaud-Vanneau A., Arnaud H., Adatte T. and Föllmi K.B., 2013. Paleoclimatic and paleoenvironmental change across the Berriasian-Valanginian boundary along a transect from the Jura platform to the Vocontian Basin. *Sedimentology*, **60**, 36–63.

Ogg J.G., Steiner M.B., Olóriz F. and Tavera J.M., 1984. Jurassic magnetostratigraphy, 1. Kimmeridgian-Tithonian of Sierra Gorda and Carcabuey, southern Spain. *Earth Planet. Sci. Lett.*, **71**, 147–162.

Ogg J.G. and Lowrie W., 1986. Magnetostratigraphy of the Jurassic/Cretaceous boundary. *Geology*, **14**, 547–550.

Ogg J.G., Hasenyager R.W., Wimbledon W.A., Channell J.E.T. and Bralower T.J., 1991. Magnetostratigraphy of the Jurassic-Cretaceous boundary interval - Tethyan and English faunal realms. *Cret. Res*., **12**, 455–482.

Pruner P., Houša V., Olóriz F., Košták M., Krs M., Man O., Schnabl P., Venhodová D., Tavera J.M. and Mazuch M., 2010. High-resolution magnetostratigraphy and biostratigraphiczonation of the Jurassic/Cretaceous boundary strata in the Puerto Escaño section (southern Spain). *Cret. Res.*, **31**, 192–206.

Příhoda K., Krs M., Pešina B. and Bláha, J., 1989. MAVACS - a new system creating a nonmagnetic environment for palaeomagnetic studies. *Cuad. Geol. Ibérica*, **12**, 223–250.

Satolli S., Turtu A. and Donatelli U., 2015. Magnetostratigraphy of the Salto del Cieco section (Northern Appenines, Italy) from the Pliensbachian to Jurassic/Cretaceous boundary. *Newsl. Stratigr.*, **48**, 153–177.

Wimbledon W.A.P., 2014. Warsaw remarks - Berriasian progress. *Volumina Jurassica*, **12(1)**, 107–112.

Wimbledon W.A.P. Casellato C.E., Reháková D., Bulot L.G., Erba E., Gardin S., Verreussel R.M.C.H., Munsterman D.K. and Hunt C.O., 2011. Fixing a basal Berriasian and Jurassic-Cretaceous (J-K) boundary - is there perhaps some light at the end of the tunnel? *Riv. Ital. Paleontol. Stratigr.*, **117**, 295–307.

Wimbledon W.A.P., Reháková D., Pszczółkowski A., Cassellato C.E., Halásová E., Frau C., Bulot L.G., Grabowski J., Sobień K., Pruner P., Schnabl P. and Čížková, K., 2013. A preliminary account of the bio- and magnetostratigraphy of the Upper Tithonian-Lower Berriasian interval at Le Chouet, Drôme (SE France). *Geol. Carpath.*, **64**, 437–460.

Zakharov V.A., Rogov M.A., Dzyuba O.A., Žák K., Košťák M., Pruner P., Skupien P., Chadima M., Mazuch M. and Nikitenko B.L., 2014. Palaeoenvironments and palaeoceanography changes across the Jurassic/Cretaceous boundary in the Arctic Realm: case study of the Nordvik section (North Siberia, Russia). *Polar Res.*, **33**, 19714, DOI: 10.3402/polar.v33.19714.